



Available at
<http://pvamu.edu/aam>
Appl. Appl. Math.
ISSN: 1932-9466

Applications and Applied
Mathematics:
An International Journal
(AAM)

Vol. 6, Issue 1 (June 2011) pp. 304 - 322
(Previously, Vol. 6, Issue 11, pp. 2045 – 2063)

Analysis of Flow Fields in a Flexible Tube with Periodic Constriction

Swati Mukhopadhyay, Prativa Ranjan De,
Mani Shankar Mandal and G.C. Layek*

Department of Mathematics
The University of Burdwan
Burdwan-713104, W.B., India
swati_bumath@yahoo.co.in
goralayek@yahoo.com; math_gclayek@buruniv.ac.in

Received: June 10, 2010; Accepted: April 7, 2011

* Author for correspondence

Abstract

Numerical techniques based on pressure-velocity formulation have been adopted to solve approximately, the governing equations for viscous flows through a tube (simulating an artery) with a periodic constriction. The effect of the constriction as well as the rigid of the tube, on the flow characteristics, and its consequences for arterial disease is the focus of this investigation. The unsteady incompressible Navier-Stokes equations are solved by using the finite-difference technique in staggered grid distribution. The haemodynamic factors like wall shear stress, pressure and velocity are analyzed through their graphical representations. Maximum resistance is attained in case of rigid stenosed tube rather than the flexible one. The main result is to contribute that the recirculating region is larger in case of a rigid tube than that of flexible one.

Key words: Periodic constriction, pressure-velocity approach, complaint wall, finite difference scheme

MSC 2010 No.: 76D, 74S20

1. Introduction

In recent past, the study of bio-fluid dynamics has become quite interesting to many researchers from the theoretical, experimental as well as the clinical point of view. Coronary artery disease, the largest single cause of mortality in developed nations occurs when the coronary arteries narrow down to the extent that they are unable to transport sufficient blood to the heart muscle for it to function efficiently. The two main causes of death from coronary artery disease are rupture of the plaque causing sudden occlusion of the artery and the slow build up of a stenosis in the artery due to atherosclerosis, a disease characterized by the hardening and thickening of the arterial walls due to formation of plaque. Reduction in blood flow caused by stenosis build up also causes debilitation. Haemodynamic is suspected to be involved in arterial lesions leading to the malfunction of the cardiovascular system resulting from the flow disturbances around bends, curvatures, tapering, and stenoses in larger arteries where plaques are frequently formed. Flow through arteries is complicated by the formation of atherosclerotic plaques on the arterial wall which impede the flow through the artery and which may substantially affect the wall shear stress distribution. Therefore, understanding blood flow through stenosed tube is of particular interest.

The ability to describe the flow through stenosed vessels would provide the possibility of diagnosing the disease in the earlier stages, even before the stenosis become clinically relevant, and is the basis for surgical intervention. Numerical simulation to predict flow through atherosclerotic arteries augment the percipience and experience of cardiologists and assist understanding of the genesis and progression of stenosis development. Such techniques allow predicting the haemodynamic characteristics as pressure, shear stress, velocity and reduction in flow. Quite a good number of theoretical and experimental investigations related to blood flow in arteries in the presence of stenosis [see Johnston et al. (2004), Chen and Lu (2006), Wiwatanapataphee et al. (2006), Jhonston and Jhonston (2008), Srivastava et al. (2010), Wong et al. (2010)] have been carried out with various perspectives in the realm of arterial biomechanics. Some attempts to study experimentally steady and unsteady flows across a smooth stenosis can be found in Young and Tsai (1973a, b), Ahmed and Giddens (1983) etc. For a single constriction flow, numerous research investigations have been conducted [Deshpande et al. (1976), Mishra and Chakravarty (1986), Pontrelli (2001), Yakhot et al. (2005), Mandal et al. (2007), Sarifuddin et al. (2008), etc.].

Laminar flow in a periodically constricted tube has now become the popular model in varied fields such as stenosed arteries and blood oxygenators, in flow-off problems as well as in leaching and filtration in natural and artificial situations. For flow in a periodically constricted tube [Figure 1] (in our case, one generated by the surface of revolution of a cosine function about the axis of symmetry) several theoretical, numerical and experimental research works have been reported. Chow and Soda (1972) gave an asymptotic analysis for large wavelengths. Lahbabi and Chang (1986) investigated the flow field numerically. On the other hand, Deiber and Schowalter (1979), Ralph (1987), Deiber et al. (1992) and Lenewit and Auerbach (1999) performed experimental and numerical studies. Recently, Mukhopadhyay and Layek (2009) presented an analysis of flow fields in a wavy-wall tapered artery. Most of the studies regarding flow through a stenosed artery have been restricted to steady flow in cylindrical rigid pipes. When stenoses develop in human vasculature, the vessel walls in the vicinity of the stenosis are usually

relatively solid but when the distensibility of the vessel wall is inducted, they will no longer be rigid. For a flexible vessel, the stenosis cannot remain static and this feature is quite relevant to the unsteady flow mechanism under stenotic condition. However, there has been a lack of research in the area of modelling blood flows in periodically constricted flexible tube. Hence the flow in a flexible tube with periodic constriction certainly deserves special attention.

So, the objective of this study is to explore the combined effects of sinusoidal local constriction and wall-flexibility on the flow characteristics of blood regarding the flowing blood as Newtonian. The rheology of blood can best be described by Casson's relationship, in which the blood exhibits nonlinear shear stress versus rate of shear characteristics, especially at low rates of shear. However, at relatively high rate of shear, the viscosity coefficient asymptotically approaches a constant value. The assumption of Newtonian behavior of blood is acceptable for high shear rate flow, e.g., in case of flow through large arteries [Pedley (1980)].

For this investigation, which centers on the flow pattern in a rigid as well as flexible tube with periodic constriction, a stable two-stage numerical scheme is developed in axi-symmetric approximations. Staggered grid and finite difference discretization are employed in the scheme. The flow reached steady state after a sufficiently long time. The flow characteristics like flow separation, pressure drop, velocity profiles and arterial wall shear stress are also discussed at length through their graphical representations.

2. Equations of Motion

We consider an axi-symmetric and laminar separated flow in a constricted tube, constricted at the specified position. The blood flow through an axi-symmetric stenosis is simulated in two-dimensions, making use of cylindrical the co-ordinate system. Let (r^*, θ^*, z^*) be the cylindrical polar co-ordinates with z^* -axis along the axis of symmetry of the tube. The region of interest is $0 \leq r^* \leq r_0(z^*)$, $0 \leq z^* \leq L^*$ (L^* being the finite length of the tube). The incompressible two-dimensional Navier-stokes equations is used for modelling the Newtonian blood flow past multiple constrictions. Let u^* and v^* be the axial and radial velocity components respectively, p^* the fluid pressure, ρ the constant density and ν the kinematic viscosity of the fluid. Let U be the maximum inflow velocity specified in the inlet section or test section of the tube. We introduce the non-dimensional variables $t = t^*U/D_0$, $r = r^*/D_0$, $z = z^*/D_0$, $r_0(z) = r_0^*(z^*/D_0)/D_0$, $u = u^*/U$, $v = v^*/U$, $p = p^*/\rho U^2$ where D_0 is the diameter of tube in the unoccluded portion. The governing equations for incompressible fluid flow representing conservation of mass and momentum fluxes may be expressed in dimensionless variables as

$$r \frac{\partial u}{\partial z} + \frac{\partial vr}{\partial r} = 0, \quad (1)$$

$$\frac{\partial u}{\partial t} + \frac{\partial uv}{\partial r} + \frac{\partial u^2}{\partial z} + \frac{uv}{r} = -\frac{\partial p}{\partial z} + \frac{1}{\text{Re}} \left[\frac{\partial^2 u}{\partial r^2} + \frac{1}{r} \frac{\partial u}{\partial r} + \frac{\partial^2 u}{\partial z^2} \right], \quad (2)$$

$$\frac{\partial v}{\partial t} + \frac{\partial v^2}{\partial r} + \frac{\partial uv}{\partial z} + \frac{v^2}{r} = -\frac{\partial p}{\partial r} + \frac{1}{\text{Re}} \left[\frac{\partial^2 v}{\partial r^2} + \frac{1}{r} \frac{\partial v}{\partial r} + \frac{\partial^2 v}{\partial z^2} - \frac{v}{r^2} \right], \quad (3)$$

where $\text{Re} = UD_0 / \nu$ is the Reynolds number.

2.1. Boundary Conditions

Along the axis of symmetry, the normal component of velocity and shear stress vanish so that

$$\frac{\partial u(z, r, t)}{\partial r} = 0, \quad v(z, r, t) = 0 \text{ on } r = 0. \quad (4)$$

The velocity boundary conditions on the arterial wall when treated to be rigid are the usual no-slip conditions given by

$$u(z, r, t) = v(z, r, t) = 0 \text{ at } r = r_0(z), \quad (5a)$$

while those in the case of flexible wall are

$$u(z, r, t) = 0, v(z, r, t) = \frac{\partial r_0(z, t)}{\partial t} \text{ on } r = r_0(z, t). \quad (5b)$$

The governing equations of our model assume that the flow regime is laminar. This model also assumes the flow to be fully developed at the inlet test section of the tube where the inlet section is considered at the position $z = 0$. The inlet velocity conditions are assumed to have a parabolic profile corresponding to Hagen-Poiseuille flow through a long circular tube as

$$u(z, r, t) = 2(1-r^2), \quad v(z, r, t) = 0 \text{ at } z = 0. \quad (6)$$

The downstream length (60) is sufficiently long so that the reattachment length is independent of the length of calculation domain. The zero velocity gradient boundary conditions are used at the outlet cross-section of the tube

$$\frac{\partial u(z, r, t)}{\partial z} = 0, \quad \frac{\partial v(z, r, t)}{\partial z} = 0. \quad (7)$$

2.2. Initial Condition

The initial condition is that there is no flow inside the region of the tube except the parabolic velocity profile at the inlet. The flow is gradually increasing as time elapses.

2.3. Transformation of Basic Equations

We consider a co-ordinate stretching in the radial direction which transforms the constricted tube into a straight circular tube, given by

$$R = \frac{r}{r_0(z)}, \quad 0 < r < r_0 \quad (8)$$

where the function $r_0(z)$ is defined as

$$r_0(z) = \begin{cases} R_0 + A \cos(2\pi \frac{z}{\lambda}), & z_1 \leq z \leq z_2 \\ 1, & \text{otherwise.} \end{cases} \quad (9)$$

Here $r_0(z)$ denotes the radius of the tube in the constricted region, $R_1 = (R_0 - A)$ is the minimum radius of the tube, $A = \gamma\lambda$ is the amplitude, $R_1 = \delta\lambda$, λ is the wave length, γ, δ are two dimensionless parameters. Here z_1 is the distance from the start of the segment to the start of the stenosis, z_2 is the distance from the start of the segment to the end of the stenosis.

All the profiles, given by equation (9) appear to be time-independent (rigid) and their time-dependence can easily be introduced in such a way that $r_0(z, t) = r_0(z) \cdot a_1(t)$ where $a_1(t) = 1 + k \cos(\omega t - \phi)$ with the amplitude parameter k , the phase angle ϕ and the angular frequency ω .

A schematic diagram of the periodically constricted tube geometry considered in this analysis is given in Fig.1 (a) along with all relevant quantities. The tube under consideration is taken to be of finite length 60 for low Reynolds number flow. But suitable length is taken for the case of high Reynolds numbers so that the reattachment length is independent of this downstream distance.

3. Numerical Computations

The primitive variable approach that is pressure-velocity formulation is adopted to solve approximately the governing transformed equations along with the boundary conditions. In this approach, velocity components are stored staggered with respect to the pressure variable [see Harlow and Welch (1965)]. This type of storing arrangement is used mainly to prevent the decoupling tendency of the pressure and known as checker-board effect in literature. The boundary conditions on pressure are not required when the velocities are prescribed on the boundary. This is not possible when non-staggered meshes are employed for discretizing the governing equations of fluid flow. The locations of the velocity components are at the centre of the cell faces to which they are normal and the pressure field at the center of the cell. If a uniform grid is used, the locations are exactly at the midway between the grid points. Finite-difference discretization of the equations (6)-(8) have been carried out.

The discretization procedures of different terms are as follows. The time derivative terms are differenced according to the first order accurate two-level forward time differencing formula. The convective terms in the momentum equations are differenced with a hybrid formula consisting of central differencing and second order up winding. The diffusive terms are differenced using the three point central difference formula. The source terms are centrally differenced keeping the position of the respective fluxes at the centers of the control volumes. The pressure derivatives are represented by forward difference formulae. Actually, the numerical algorithm consists of two stages. In the first stage, the pressure Poisson equation (derived from the momentum equations and the mass conservation equation) are solved to obtain the approximate value of pressure field and then updates two momentum equations using known pressure field and previous level velocity vector. Pressure-velocity corrections formulae are then invoked in the second stage of the numerical scheme. This correction scheme is also derived using momentum and continuity equations [Layek et al. (2005)]. This scheme is very much effective for achieving the desired level of accuracy in the mass conservation equation (the main constraint of incompressible Navier-Stokes equations) at each cell. The detailed derivation and numerical algorithm are given in Layek et al. (2005).

The pressure equation is solved iteratively, by the SOR (successive over-relaxation) method and the corresponding boundary conditions have been implemented properly. After performing a few iteration steps with the pressure equation, the pressure-velocity corrections are invoked. The method is continued until it achieves a satisfactory level of divergence value (in this case, we fixed the divergence value at 0.00001).

3.1 Stability Criteria of the Scheme

The time-step (δt) is calculated by the two criteria given below. First the fluid cannot move through more than one cell in one time step (Courant, Friedrichs and Lewy condition). So the time step must satisfy the following criteria

$$\delta t \leq \text{Min} \left[\frac{\delta z}{|u|}, \frac{\delta R}{|v|} \right]_{ij}, \quad (10)$$

where minimum is taken in the global sense. Secondly, momentum must not diffuse more than one cell in one time step. This condition, which is related to the viscous effects, implies

$$\delta t \leq \text{Min} \left[\frac{\text{Re}}{2} \frac{\delta z^2 \delta R^2}{(\delta z^2 + \delta R^2)} \right]_{ij}. \quad (11)$$

Denoting the right hand side of (10) and (11) by δt_1 and δt_2 respectively we find that both these inequalities are satisfied if the time step δt satisfies

$$\delta t \leq \text{Min}[\delta t_1, \delta t_2]. \quad (12)$$

Hence, in our computations we take

$$\delta t = c \text{Min}[\delta t_1, \delta t_2], \quad (13)$$

where c is a constant lying between 0.2 to 0.4. A typical value of δt is 0.005 for $\delta z = 0.05$ and $\delta R = 0.05$.

4. Results and Discussions

For the purpose of numerical computation of the desired quantities of major physiological significance, numerical values of the specific geometry of the stenosed artery considered for simulations and the parameters involved in this study are ranged around some typical values in order to obtain results of physiological interest:

$$z_1 = 10.1, z_2 = 38, \lambda = 9.62, \gamma = 0.0225, \delta = 0.06, k = 0.001, \quad [\text{for model-1 (i.e. for constriction-height } 0.4)]$$

$$\omega = 2\pi \times 1.2 \text{ Hz}, \phi = 180^\circ.$$

Using the above numerical algorithm, we compute the stream function (ψ) and vorticity (ω) for different values of R of a long straight circular tube at the Reynolds number $Re = 10$ for the grid size 600×20 . The values are compared with the exact values of ψ and ω and prescribed in the following Table 1.

Table 1. Results of stream function ψ and vorticity ω for a long circular tube at $Re=10$.

Property	$R \rightarrow 0$	0.25	0.50	0.75	1
Computed ψ	0.0	0.03027	0.10938	0.20215	0.25002
Exact ψ	0.0	0.03027	0.10938	0.20215	0.25000
Computed ω	0.0	0.49996	0.99994	1.49990	1.99982
Exact ω	0.0	0.50000	1.00000	1.50000	2.00000

Table 1 shows that the computed values of stream function and vorticity agree well with their exact values for the case of straight circular tube. The value of wall shear stress is found to be 1.99 against the exact value 2 for laminar flow in a tube under constant pressure gradient. Thus, our numerical code has been validated by simulating the flow in a straight tube.

The present results involving the pressure drop in case of irregular stenosis for different Reynolds number from 10 to 1000 are compared with the experimental results of Back et al. (1984) and the numerical results of Andersson et al. (2000), Sarifuddin et al. (2008) in Figure 1(b). The comparison in Figure 1 (b) shows considerable agreement with the experimental results of Back et al. (1984) and numerical results of Sarifuddin et al. (2008). But there is a little variation with the numerical results of Andersson et al. (2000). It seems that the unsteady flow mechanism of the present investigation is responsible for this.

The computed results are obtained following the above mentioned numerical scheme [taking $\delta t = 0.005$ for $\delta z = 0.05$ and $\delta R = 0.05$] for various physical quantities of major physiological significance. In order to have their quantitative measures they are all exhibited through the Figures 2-7 and discussed at length.

The arterial wall distensibility is disregarded in some cases (for rigid tube) but attention also has been paid on compliant wall model.

Wall pressure distribution is very much important because the post-stenotic dilatation due to arterial damage is caused by the variation of pressure associated with the complex flow structure. Pressure fluctuations on the arterial wall produce acoustic signals that can be detected externally [Mittal et al. (2001)].

Wall pressure distribution at the surface of the periodic constriction for rigid walled tube and for flexible walled tube are presented in Figure 2(a) and Figure 2(b), respectively, for constriction height $R_0 = 0.4$ and at $Re = 700$. The pressure gradient is found to vary over the cross sections in both cases. The pressure distribution curve (in both cases) shows a rapid fall as the flow approaches the indentation as well as near the second and third area reductions but the pressure gradient decreases sharply near the first area reduction than that in the other two cases and recovers its value after first, second and third area reductions. The local minimum is attained corresponding to the separation point in case of rigid [Figure 2(a)] as well as in flexible tube [Figure 2(b)]. The two curves are of similar nature. The profile for the lowest pressure corresponds to the maximum mean velocity and that for the high pressure corresponds to the minimum mean velocity. Low pressure around the stenotic portion generates a health risk because the stenosed arteries may collapse due to low pressure [Tang et al. (2001)].

In presence of a narrowing i.e. a constriction, the flow exhibits a resistance and hence an increase of the shear stress (i.e., the wall vorticity) and a pressure drop occur. These are quantities of physiological relevance.

The viscous effect on the pressure drop is also important, particularly in front of the throats of the tube. Keeping this in mind, a quantitative analysis, for instance the pressure drop as functions of Reynolds number and the geometric parameter - height of the constriction (R_0) are investigated.

Comparison of the pressure drop curves over the rigid and flexible walled constricted tubes show that the flexible tube predicts higher pressure drop than the rigid one for low Reynolds number [Figure 3(a)] but at higher Reynolds number the pressure drop is higher in case of rigid tube than

that of flexible one. The non-dimensional pressure drop in a flexible constricted tube for two different constriction heights ($R_0 = 0.4, 0.6$) is presented in Figure 3(b). This figure shows that flow in a severely constricted artery produces a higher pressure drop, i.e., when the height of the constriction increases, amount of pressure drop also increases. With increasing degree of stenosis, the reduction in pressure at the throat decreases significantly.

Figure 4(a) exhibits the variation of center line velocity in axial direction at $Re = 500$ in case of periodically constricted rigid as well as flexible artery for constriction height $R_0 = 0.4$. It is very clear from the figure that the maximum centre line velocity occurs slightly in the downstream of the constriction (for rigid as well as flexible artery) due to formation of recirculation zone near the wall as a result of flow separation. Flexible artery induces excess flow acceleration as compared to rigid artery. It is noted that the centre line velocity takes a larger distance to recover its initial value as Reynolds number increases.

The unsteady response of the flow phenomena through distensible artery seems to have major significance in realistic blood flow under stenotic condition. Keeping this in mind the behavior of stream wise velocity component with time for $Re = 700$, at $z = 11$ (where z is the distance from the inlet of the tube) (i.e., in the constricted region) for constriction height $R_0 = 0.6$ for both rigid and flexible arteries is exhibited in Figure 4(b). Both the rigid and flexible arteries experience large distortions on stream wise velocity component at the onset of time followed by uniformly undulating stream wise velocity in case of rigid artery and an uniform stream wise velocity for the flexible one for rest of the time considered here.

The velocity profiles are of some interest since they provide a detailed description of the flow field. The velocity profiles are plotted in Figure 5(a) [for rigid tube] and in Figure 5(b) [for flexible tube] for several axial positions at $Re = 700$ and for constriction height $R_0 = 0.4$. The region of reversal flow is evidenced in these two Figures. In this region, the components of velocity undergo a change in sign. It is found that the back flow region is longer in case of a rigid constricted artery than that of flexible one.

Wall shear stress is an important factor to be studied as it plays an important role in the creation and proliferation of arteriosclerosis. The principle features of the can also be determined by examining the wall shear stress. High wall shear stress may damage the vessel wall and is the cause of the intimal thickening. So wall shear stress is of physiological importance. No reliable method seems to be available for computing wall shear stress. In this situation, the numerical simulation provides some insight into the level of the wall shear stress involved.

Figure 6(a) is the graphical representation of wall shear stress for several values of Reynolds number in a flexible artery of constriction height $R_0 = 0.4$. From the figure it is noticed that no separation takes place at $Re = 50$. It is also seen that the location of the peak vorticity occurs just before the minimum constriction plane (for both rigid and flexible wall models). The magnitude of the wall shear stress values increase rapidly when the flow approaches to the constriction and reaching a peak value near the minimum constriction plane in all cases. At a location downstream of this, the wall shear stress decreases rapidly and reverses to negative values when separation begins at the wall of the tube. The places of zero vorticity are the locations of

stagnation points as well as the separation and reattachment points of the attached vortices. It is also noted that the peak value of wall shear stress decreases near the second and third area reductions. The peaks of the shear stresses are believed to cause severe damage to the arterial lumen which in turn helps in detecting the aggregation sites of platelets may have several consequences in circulatory system. This figure also displays that length of separation increases in the downstream of the constriction.

Figure 6(b) exhibits the effect of increasing the severity of the stenosis on flexible artery at $Re = 250$. Peak value of wall shear stress and the length of separation zone increase as the height of the constriction increases. Separation zones after the first and second area reductions are practically equal but larger separation zone is noticed after the third area reduction which clearly indicates the presence of a strong eddy after the last area reduction than the previous area reductions. Same nature of wall shear stress is observed in case of rigid tube.

For both rigid and flexible arteries [Figure 7(a)], an almost similar trend is observed in the respective distributions of wall shear stress differing in magnitudes only. Peak value of wall shear stress is maximum in case of rigid tube rather than that of flexible one. Here, the point of reattachment is shifted further towards downstream after the first and second area reductions in case of flexible tube compared to that of rigid tube but after the third area reduction (i.e., after the end of the constriction) opposite behavior is noticed [Figure 7(b)].

5. Conclusion

Flow through flexible periodically constricted artery is analyzed by numerical simulation of viscous incompressible fluid in a 2D vessel with the approximation of axial symmetry of the flow. The present model would certainly give better insight into the complex flow phenomena in the stenotic conditions. Potential improvement is made by the incorporation of vessel wall distensibility. The development of the separation zones towards the diverging section of the constriction is believed to be the prime areas for further deposition of atherosclerotic plaques.

Acknowledgement

Thanks are due to the honorable reviewers for their constructive suggestions which helped a lot to improve the quality of the paper.

REFERENCES

Ahmed, A.S. and Giddens, D.P. (1983). *Velocity measurements in steady flow through axisymmetric stenosis at moderate Reynolds numbers*, J. Biomech., 16, pp. 505-516.

- Andersson, H.I., Halden, R. and Glomsaker, T. (2000). *Effect of surface irregularities on flow resistance in differently shaped arterial stenoses*, J. Biomech., 33, pp. 1257-1262.
- Back, L.H., Cho, Y.I., Crawford, D.W., and Cuffel, R.F. (1984). *Effects of mild atherosclerosis on flow resistance in a coronary artery casting of man*, ASME J. of Biomech. Eng., 106, pp. 45-83.
- Chen, J. and Lu, X.Y. (2006). *Numerical investigation of the non-Newtonian pulsatile blood flow in a bifurcation model with a non-planar branch*. J. Biomech., 39, No. 5, pp.818-832.
- Chow, J.C.F. and Soda, K. (1972). *Laminar flow in tubes with constriction*, Phys. of Fluids, 15, pp.1700-1706.
- Deiber, J.A. and Schowalter, W.R. (1979). *Flow through tubes with sinusoidal axial variations in diameter*, AIChE J., 25, pp. 638-644.
- Deiber, J. A., Peirotti, M.B., Bortolozzi, R.A. and Durelli, R.J. (1992). *Flow of Newtonian fluids through sinusoidally constricted tubes. Numerical and experimental results*, Chem. Engng. Comm., 117, pp. 241-262.
- Deshpande, M.D., Giddens, D.P. and Mabon, R.F. (1976), *Steady laminar flow through modeled vascular stenoses*, J. Biomech. 9, pp. 165-174.
- Harlow, F.H. and Welch, J.E. (1965). *Numerical calculation of time dependent viscous incompressible flow of fluid with free surface*, Phys. Of Fluids, 8, pp. 2182-2189.
- Johnston, B.M., Johnstona, P.R., Corneyb, S., and Kilpatrick, D. (2004). *Non-Newtonian blood flow in human right coronary arteries: Steady state simulations*. J Biomech., 37, pp. 709-720.
- Jhonston, P.R. and Jhonston, B.M. (2008). *Blood flow in S-shaped in-plane and out- of-plane coronary arteries*, ANZIAM J., 49 (EMAC2007), pp. C341-C358.
- Lahbabi, A. and Chang, H.C. (1986). *Flow in periodically constricted tubes: transition to inertial and non-steady flows*, Chem. Engng. Sci., 41, pp.2487-2505.
- Layek, G.C., Mukhopadhyay, S. and Samad, A.S. (2005). *Oscillatory flow in a tube with multiple constrictions*, Int. J. of Fluid Mech. Research, 32, No.4, pp.402-419.
- Lenewit, G. and Auerbach, D. (1999). *Detachment phenomena in low Reynolds number flows through sinusoidally constricted tubes*, J. Fluid Mech., 387, pp.129-150.
- Mandal, P. K., Chakravarty, S. and Mandal, A. (2007). *Numerical study of the unsteady flow of non-Newtonian fluid through differently shaped arterial stenoses*. Int. J. of Comput. Mathe., 84, NO. 7, pp. 1059-1077.
- Misra, J.C. and Chakravarty, S. (1986). *Flow in arteries in presence of stenosis*, J. Biomech., 19, pp. 907-918.
- Mittal, R., Simmons, S. P., and Udaykumar, H.S. (2001). *Application of large-eddy simulation to the study of pulsatile flow in a modeled arterial stenosis*, J. of Biomech. Eng. ASME, 123, pp. 325-332.
- Mukhopadhyay, S. and Layek, G.C. (2009). *Analysis of flow fields in a wavy- walled tube with tapering*, Chinese J. of Physics, 47, No. 4, pp. 479-493.
- Pedley, T.J. (1980). *The Fluid Mechanics of large blood vessels*, Cambridge University Press.
- Pontrelli, G. (2001). *Blood flow through an axisymmetric stenosis*, Proceedings of the Institution of Mechanical Engineers, Part H: Journal of Engineering in Medicine, 215, No.1, pp. 1-10.
- Ralph, M.E. (1987). *Steady flow structures and pressure drops in wavy-walled tubes*, Trans. ASME J. Fluids Engng., 109, pp. 255-261.

- Sarifuddin, Chakravarty, S., Mandal, P.K., and Layek, G.C. (2008). *Numerical simulation of unsteady generalized Newtonian blood flow through differently shaped distensible arterial stenoses*. J. of Medical Eng. & Tech., 32, No. 5, pp. 385–399.
- Srivastava, V.P., Mishra, S., and Rastogi, R. (2010). *Non-Newtonian arterial blood flow through an overlapping stenosis*, Applications and Applied Mathematics: An Int. J. (AAM), 5, No.1, pp.225-238.
- Tang, D., Yang, C., Kobayashi, S. and Ku, D. N. (2001). *Generalized finite difference method for 3-D viscous flow in stenotic tubes with large wall deformation and collapse*, Applied Numerical Mathematics, 38, pp. 49.
- Wiwatanapatapee, B., Poltem, D., Wu, Y.H., and Lenbury, Y. (2006). *Simulation of pulsatile flow of blood in stenosed coronary artery bypass with Graft*, Mathematical Biosciences and Engineering, 3, No.2, pp. 371-383.
- Wong, K., Tu, J., Mazumdar, J., Abbott, D. (2010). *Modelling of blood flow resistance for an atherosclerotic artery with multiple stenoses and poststenotic dilatations*, ANZIAM J., 51 (EMAC2009), pp. C66-C82.
- Yakhot, A., Grinberg, L. and Nikitin, N. (2005). *Modeling rough stenoses by an immersed-boundary method*, Journal of Biomechanics, 38, pp. 1115–1127.
- Young, D.F., and Tsai, F.Y. (1973a). *Flow characteristics in models of arterial stenoses-I, Steady flow*, J. Biomech., 6, pp. 395-410.
- Young, D.F., and Tsai, F.Y. (1973b). *Flow characteristics in models of arterial stenoses-II, Steady flow*, J. Biomech., 6, pp. 547-559.

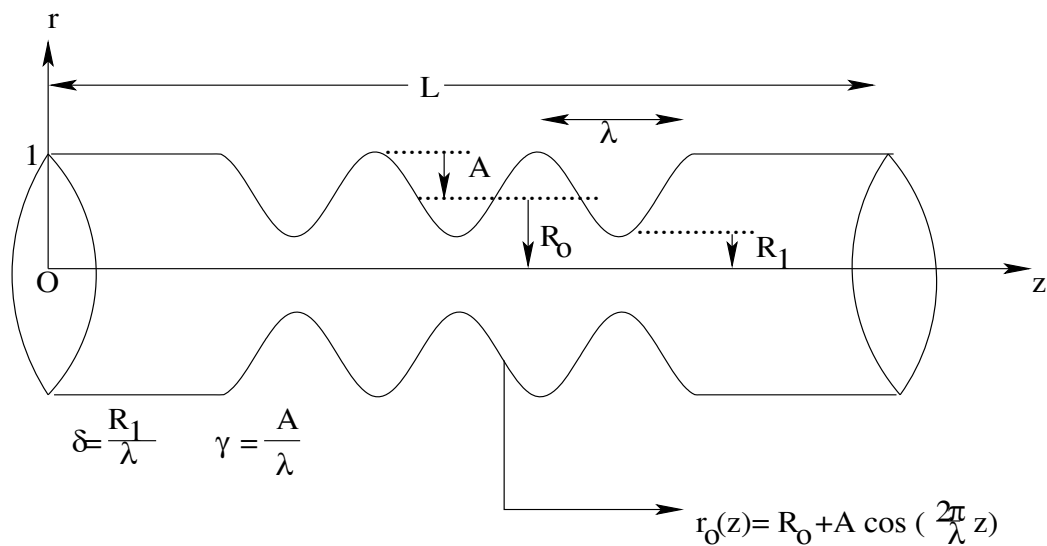


Fig.1(a): Geometry of the periodically constricted tube

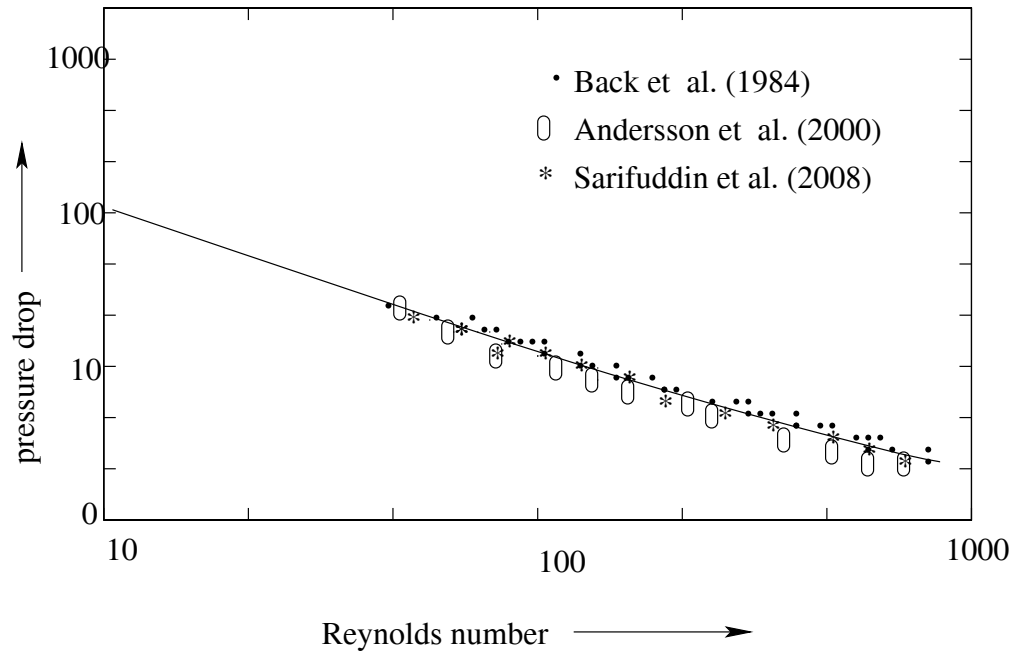


Fig. 1(b): Comparison of nondimensional pressure drop.

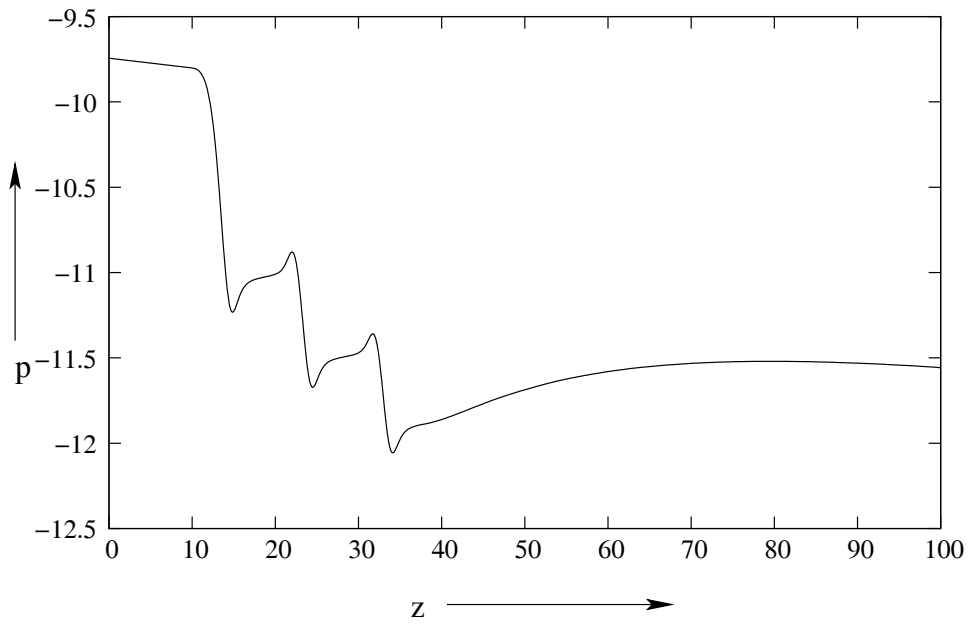


Fig. 2(a): Wall pressure distribution in a rigid tube with periodic constriction of height $R_0=0.4$ and at $Re=700$.

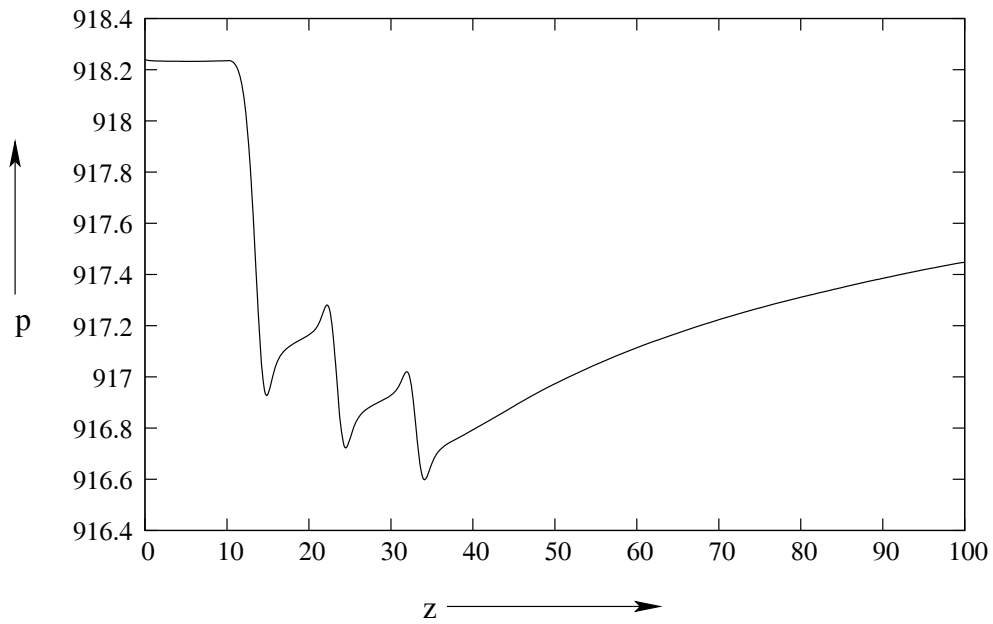


Fig. 2(b): Wall pressure distribution in a flexible tube with periodic constriction of height $R_0=0.4$ and at $Re=700$.

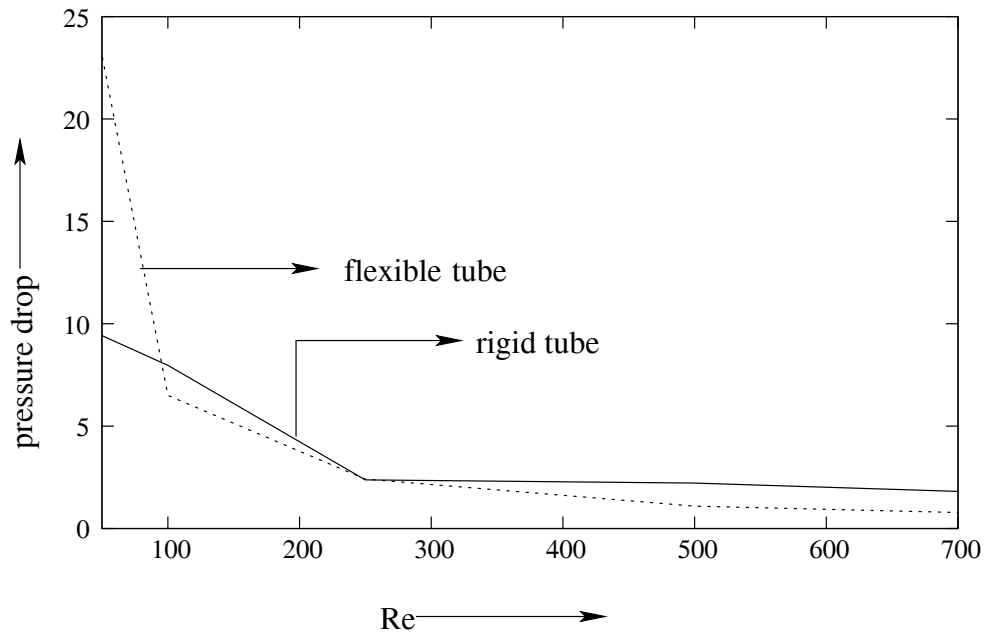


Fig. 3(a): Pressure drop in a rigid as well as flexible tube with periodic constriction of same height $R_0=0.4$.

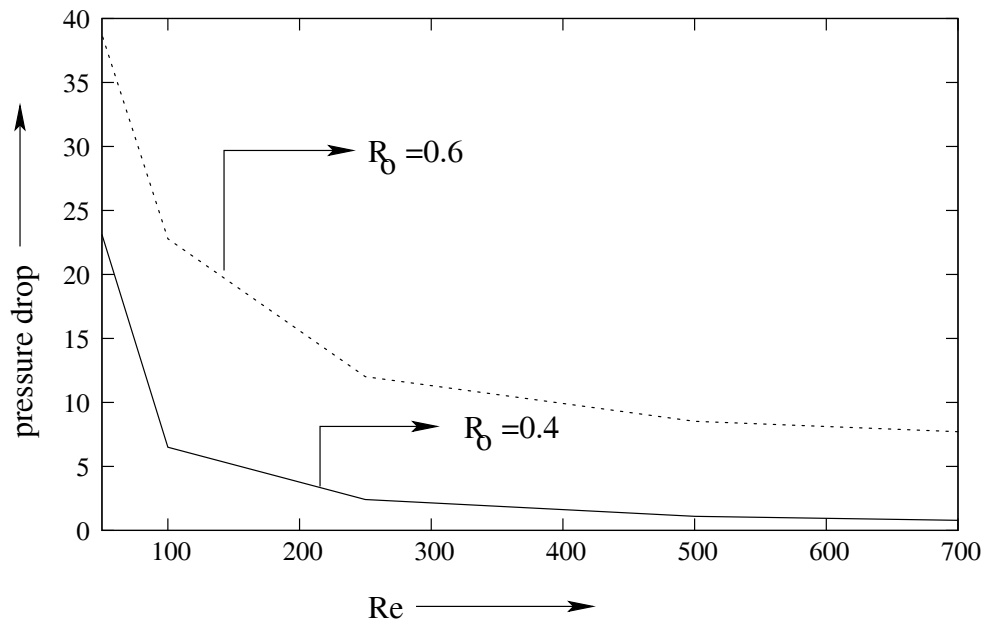


Fig. 3(b): Pressure drop in a flexible tube with periodic constriction for two different heights.

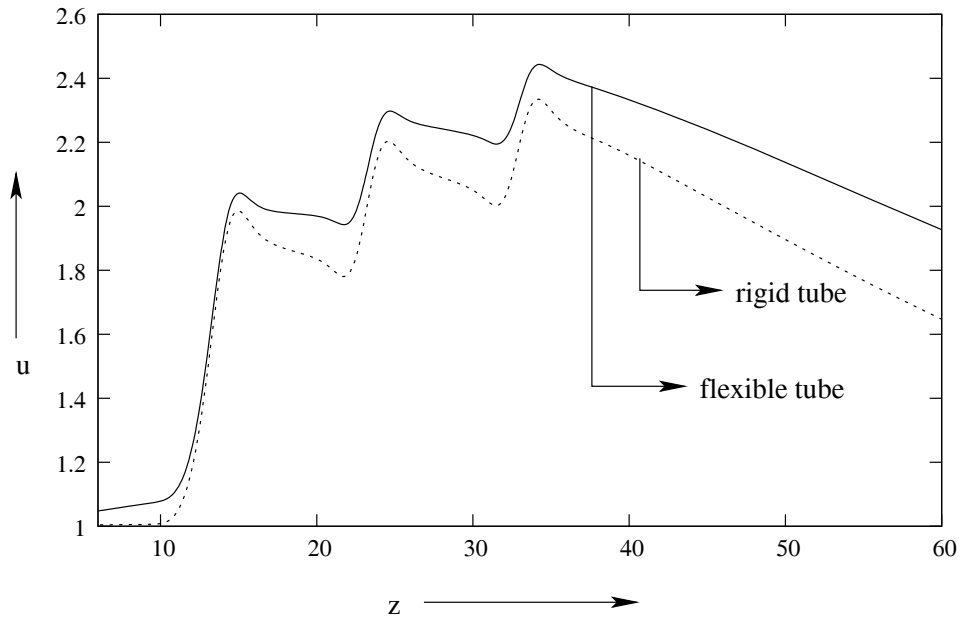


Fig. 4(a): Centre line u -velocity distribution in a rigid as well as flexible tube with periodic constriction of height $R_0=0.4$ at $Re=500$.

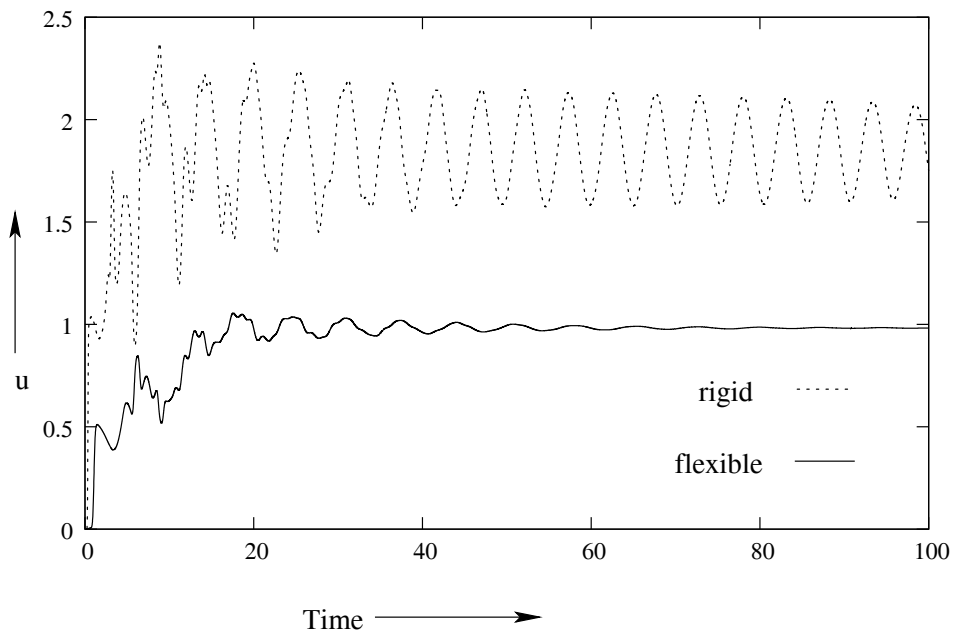


Fig.4(b): Time history of streamwise velocity component at $Re=700$ in a rigid as well as flexible tube with periodic constriction of height $R_0=0.6$ at $z=11$ (in the constricted region).

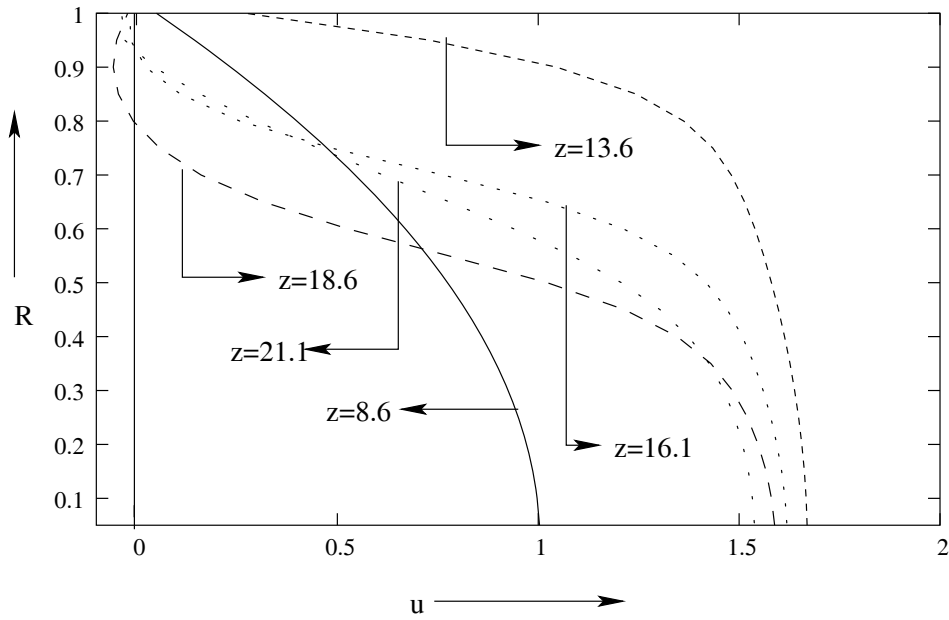


Fig. 5(a): Velocity profiles for several axial positions z where z is the distance from the inlet test section of a rigid tube with periodic constriction of height $R_0 = 0.4$ at $Re=700$.

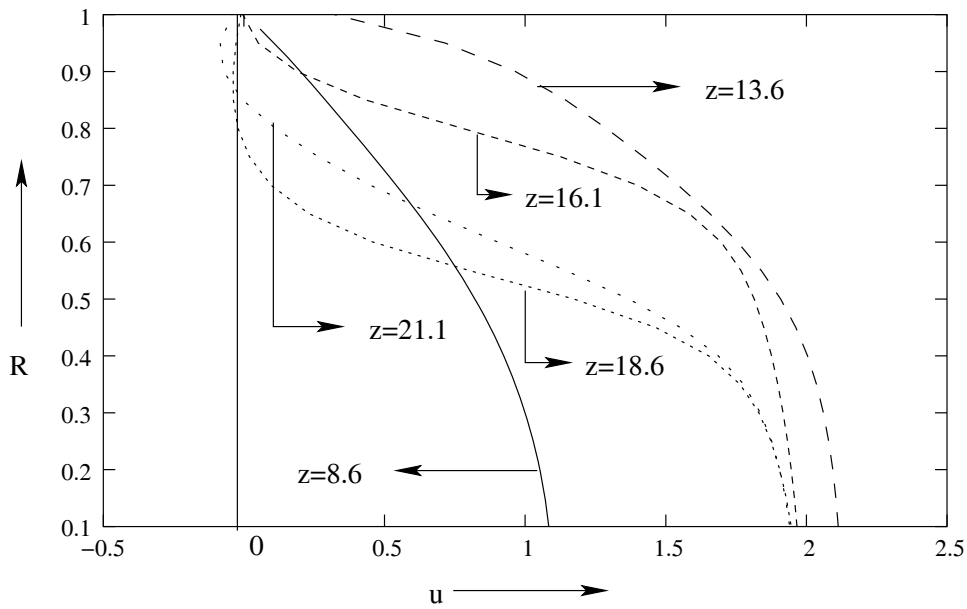


Fig. 5(b): Velocity profiles for several axial positions z where z is the distance from the inlet test section of a flexible tube with periodic constriction of height $R_0 = 0.4$ at $Re=700$.

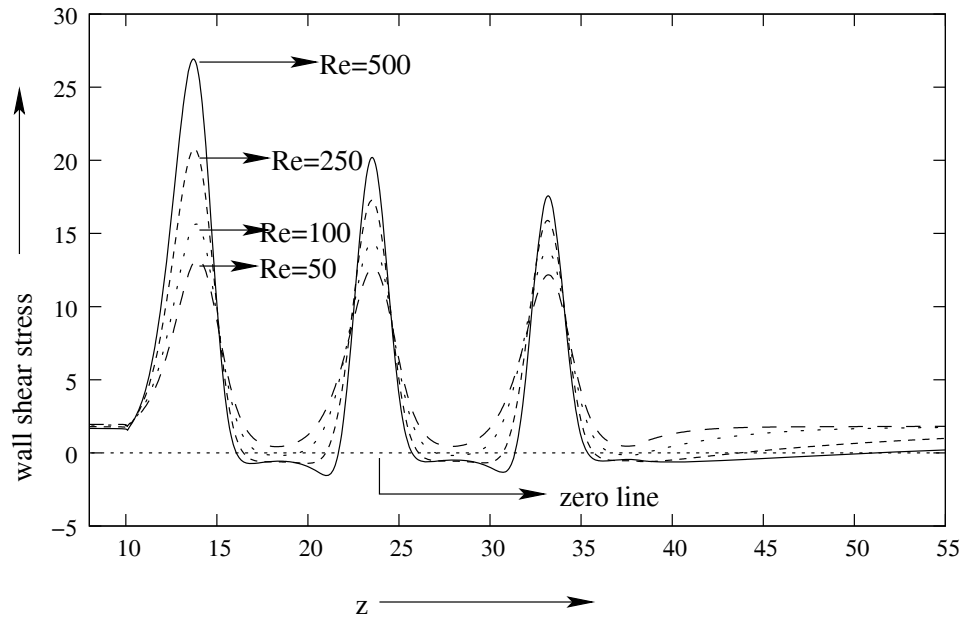


Fig. 6(a): Wall shear stress distribution in a flexible tube with periodic constriction of height $R_0 = 0.4$ for several values of Reynolds number.

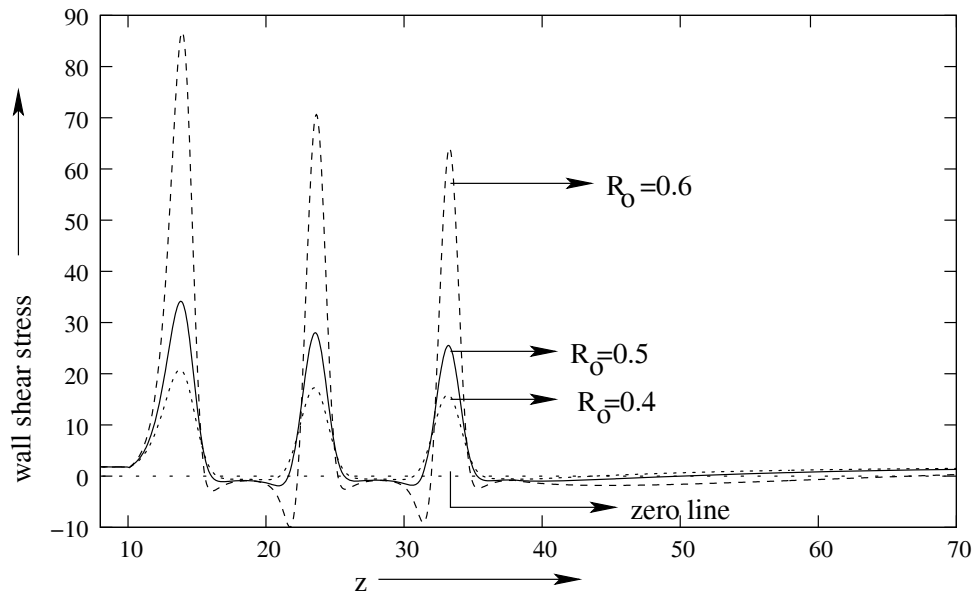


Fig. 6(b): Wall shear stress distribution in a flexible tube with periodic constriction of several heights at $Re = 250$.

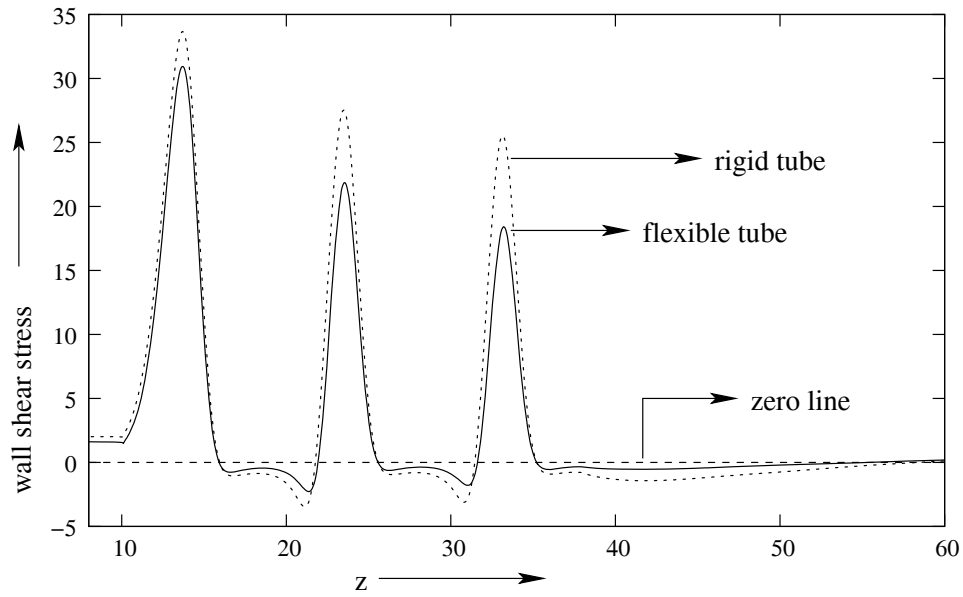


Fig. 7(a): Wall shear stress distribution in a rigid as well as a flexible tube with periodic constriction of height $R_0=0.4$ at $Re=700$.

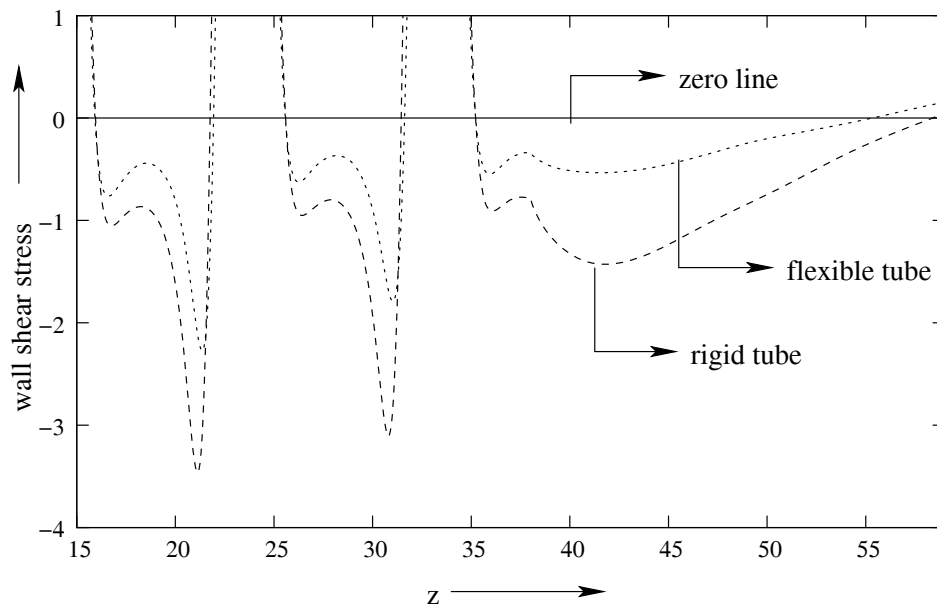


Fig. 7(b): Separation and reattachment points for flow in a rigid as well as a flexible tube with periodic constriction of height $R_0=0.4$ at $Re=700$.